RESEARCH ARTICLE

Brain
Pathology

Targeting autotaxin impacts disease advance in the SOD1-G93A mouse model of amyotrophic lateral sclerosis

Ángela Gento-Caro | Esther Vilches-Herrando | Federico Portillo |
David González-Forero [ORCID] | Bernardo Moreno-López [ORCID]

GRUpo de NEuroDEgeneración y
NeurorREparación (GRUNEDERE),
Área de Fisiología, Facultad de Medicina,
Universidad de Cádiz-Instituto de
Investigación e Innovación Biomédica de
Cádiz (INiBICA), Cádiz, Spain

Correspondence
Bernardo Moreno-López and
David González-Forero GRUpo de
NEuroDEgeneración y NeurorREparación
(GRUNEDERE), Área de Fisiología,
Facultad de Medicina, Universidad
de Cádiz-Instituto de Investigación
e Innovación Biomédica de Cádiz
(INiBICA), Plaza Falla 9, Cádiz 11003,
Spain.
Email: bernardo.moreno@uca.es (B. M-L.)
and david.gonzalezforero@uca.es (D. G-F.)

Funding information
BFU2015-71422-R (MINECO/FEDER)
from Spain's Government; FEDER-
UCA18-108475 from the 2014–2020
ERDF Operational Programme and the
Department of Economy, Knowledge,
Business and University of the Regional
Government of Andalusia; LI19/10IN-
CO21 from INiBICA to BML and PID2019-
110960GB-I00 (MICINN) from Spain's
Government to BML and DGF

Abstract

A preclinical strategy to broaden the search of potentially effective treatments in amyotrophic lateral sclerosis (ALS) relies on identifying factors controlling motor neuron (MN) excitability. These partners might be part of still unknown pathogenic pathways and/or useful for the design of new interventions to affect disease progression. In this framework, the bioactive membrane-derived phospholipid lysophosphatidic acid (LPA) affects MN excitability through LPA receptor 1 (LPA_1). Furthermore, LPA_1 knockdown is neuroprotective in transgenic ALS SOD1-G93A mice. On this basis, we raised the hypothesis that the major LPA-synthesizing ectoenzyme, autotaxin (ATX), regulates MN excitability and is a potential target to modulate disease development in ALS mice. We show here that PF-8380, a specific ATX inhibitor, reduced intrinsic membrane excitability (IME) of hypoglossal MNs in brainstem slices, supporting that baseline ATX activity regulates MN IME. PF-8380-induced alterations were prevented by a small-interfering RNA directed against mRNA for lpa_1. These outcomes support that impact of ATX-originated lysophospholipids on MN IME engages, at least, the G-protein-coupled receptor LPA_1. Interestingly, $mRNA_{atx}$ levels increased in the spinal cord of pre-symptomatic (1–2 months old) SOD1-G93A mice, thus preceding MN loss. The rise in transcripts levels also occurred in cultured spinal cord MNs from SOD1-G93A embryos, suggesting that $mRNA_{atx}$ upregulation in MNs is an etiopathogenic event in the ALS cell model. Remarkably, chronic administration in the drinking water of the orally bioavailable ATX inhibitor PF-8380 delayed MN loss, motor deterioration and prolonged life span in ALS mice. Treatment also led to a reduction in LPA_1-immunoreactive patches in transgenic animals mostly in MNs. These outcomes support that neuroprotective effects of interfering with ATX in SOD1-G93A mice rely, at least in part, on LPA_1 knockdown in MNs. Therefore, we propose ATX as a potential target and/or a biomarker in ALS and highlight ATX inhibitors as reasonable tools with therapeutic usefulness for this lethal pathology.

1 | INTRODUCTION

Despite the diverse aetiology of the disease, the sporadic and familial forms of amyotrophic lateral sclerosis (ALS) share excitability alterations in motor circuits as a central hallmark [1]. Early symptoms in both variants of the disease consist of fasciculation, cramps, hyper-reflexia and/or spasticity, which are commonly associated with motor neuron (MN) hyper-excitability [1–4]. In fact, hyper-excitability is a valuable diagnostic biomarker to differentiate a number of ALS-like patterns and to track disease advances in pre-symptomatic cases of familial ALS [4]. Furthermore, in the epidemiological framework, membrane hyper-excitability has been suggested as a consistent predictor for shorter survival rates in ALS patients [5]. Outstandingly, altered excitability of MNs is postulated to be causally related to their selective degeneration in ALS [2,6]. In the arena of the current debate on the deleterious/protective impact of hyper-excitability in ALS, a line of argument supports that intrinsic hyper-excitability of MNs promotes the excitotoxic route [7,8]. In this line, agents that reduce intrinsic membrane excitability (IME) were neuroprotective for MNs exposed to an excitotoxic challenge and also in ALS mice [8]. Hyper-excitability has been alternatively postulated as a beneficial transitory state in ALS, by contributing to the survival of S-type MNs, the MN subtype resistant to degeneration during disease progression [9–12]. In addition, an inconsistency with the hypothesis that hyper-excitability causes MN death in ALS is that FF-type MNs, the most vulnerable in ALS mouse models, exhibit hypo-excitability prior to degeneration [13]. Anyway, factors that impact MN excitability might represent potential targets to affect disease progression, partners in etiopathogenic mechanisms and/or biomarkers in ALS.

Against this background, the extracellular enzyme autotaxin (ATX), encoded by the ectonucleotide pyrophosphatase/phosphodiesterase 2 (*enpp2*) gene, emerges as a plausible candidate to control MN IME and, therefore, it can be postulated as a promising target to modulate disease progression in ALS. ATX is an ectoenzyme enriched in the brain with a pronounced lysophospholipase D activity, being the primary source of the lipid signalling molecule lysophosphatidic acid (LPA) [14,15]. Thus, the majority of biological effects of ATX are associated with its ability to synthesize bioactive LPA from lyso-phosphatidylcholine (LPC) which, in turn, mainly stems from the cleavage of the membrane phospholipid phosphatidylcholine (PC) by phospholipase A_2 (PLA_2) [15]. In the CNS, ATX participates in several physiological processes such as brain and oligodendrocyte development and microglial activation. However, dysregulation of the ATX-LPA axis may contribute to many CNS disorders comprising inflammation, brain cancer, multiple sclerosis and Alzheimer's disease to quote some [15]. In the context of our working hypothesis, several findings underpin that ATX could contribute to disease pathogenesis: (i) levels of PC and LPC are augmented in the ventral horn of spinal cord tissue samples obtained from ALS patients [16]; (ii) PC is, indeed, the most abundant and discriminant lipid in cerebrospinal fluid of ALS patients [17]; (iii) obesity, a condition in which the ATX-LPA axis becomes dysregulated at both, systemic and CNS levels, is a predictor of better long-term survival of ALS patients [18–20]; (iv) the most prevalent LPA receptor in MNs, LPA_1, is upregulated in the spinal cord and MNs from the transgenic SOD1-G93A mouse model of ALS preceding MN loss [21,22] and (v) interfering with LPA_1 affects MN IME and is neuroprotective in SOD1-G93A mice [22]. These findings, therefore, provide support to our main hypothesis and raise the possibility that targeting ATX could affect ALS progression.

In this report, we show that targeting ATX with an orally bioavailable specific inhibitor, PF-8380, leads to a reduction in MN IME *in vitro* by involving LPA_1 signalling. In addition, we demonstrate that $mRNA_{atx}$ is upregulated in the spinal cord of SOD1-G93A mice before MN death and in cultured MNs from SOD1-G93A embryos. Finally, we provide evidence that chronic treatment with the ATX inhibitor slows down disease progression in ALS mice by a mechanism of action, at least in part, involving LPA_1 knockdown in MNs.

2 | METHODS

Experiments were performed in neonatal (P5–P9, either sex) Wistar rats; young mice (1–2-month-old male) either SOD1-G93A (Jackson Laboratory, Bar Harbor, ME, USA) and non-transgenic (non-Tg) littermates; and embryos extracted from SOD1-G93A pregnant mice (12.5 days gestation). Animals were provided by the local Animal Supply Services (SEPA, University of Cadiz), and their care and handling followed the guidelines of the European Union Council (2010/63/EU, 86/609/UE). Experimental procedures were approved by the local Animal Care and Ethics Committee (University of Cadiz, Cadiz, Spain) and the Ministry of Agriculture, Fisheries and Rural Development (Junta de Andalucía, Spain). Animals were individually housed in cages with

water and food pellets available *ad libitum*, at 21 ± 1°C, with a 12-h light/dark cycle. All efforts were applied to minimize the number of animals used and their suffering.

2.1 | Whole-cell patch-clamp

Current-clamp recordings were performed in hypoglossal MNs (HMNs) from brainstem slices (P5–P9 rats) as previously described [22]. Briefly, pups were guillotined under anaesthesia by hypothermia (10–15 min at 4°C) and their brainstems rapidly removed and dissected in carbogen (95% O_2, 5% CO_2) bubbled artificial cerebrospinal fluid (aCSF) enriched with sucrose at 4°C (in mM: 26 $NaHCO_3$, 10 glucose, 3 KCl, 1.25 NaH_2PO_4, 2 $MgCl_2$ and 218 sucrose). Coronal slices (300–400-μm thick), obtained using a vibroslicer (NVSL; WPI), were transferred to normally oxygenated aCSF (in mM: 26 $NaHCO_3$, 10 glucose, 3 KCl, 1.25 NaH_2PO_4, 6 $MgCl_2$, 130 NaCl and 0.5 $CaCl_2$) and stabilized at ~37°C for 1 h. Slices were then relocated to a recording chamber for electrophysiological assays.

Recordings of HMNs were carried out under perfusion (~3–4 ml min^{-1}) with normally oxygenated aCSF at 31°C. The patch was performed at the HMN somata, using a Nikon (Tokyo, Japan) Eclipse CFI60 microscope equipped with an infrared differential interference contrast system. Patch pipettes (1.5–3 MΩ resistance) were filled with the following internal solution (in mM): 17.5 KCl, 122.5 K-gluconate, 9 NaCl, 1 $MgCl_2$, 10 HEPES, 0.2 EGTA, 3 Mg-ATP and 0.3 GTP-Tris at pH 7.4. Recordings were obtained and low-pass Bessel filtered at 10 kHz with a MultiClamp 700B amplifier. Data were digitized at 20 kHz with a Digidata 1332A analogue-to-digital converter and acquired using pCLAMP 10.0 software (Molecular Devices, Foster City, CA). Only cells exhibiting small (<20 MΩ) and stable (change <20%) access resistance were analysed. Series resistance was usually compensated 65–75%. The pipette offset potential was neutralized just before HMNs were patched. Recordings were not adjusted for liquid junction potential.

To analyse HMNs IME, resting membrane potential (Vm), threshold current (I_{th}), threshold for action potential (AP) generation (AP threshold) and input resistance (R_N) were measured [22]. I_{th} was determined as the lowest depolarizing current pulse (5 ms) required to evoke an AP in 50% of cases. The AP threshold was estimated as the membrane potential corresponding to 5% of the first peak amplitude in the second derivative (d^2V/dt^2) obtained from the waveform as previously described [22,23]. R_N was calculated from the current–voltage (I–V) plots obtained by injecting a series of depolarizing and hyperpolarizing current pulses (0.5 s, −0.2–0.2 nA). The resulting data points were then fitted with a regression line, and R_N was the slope of the lines.

2.2 | Quantitative real-time reverse transcriptase PCR (*q*RT-PCR)

These measures were performed following a well-established protocol in our lab [8,21,22]. Briefly, total RNA was extracted either from the lumbar spinal cord or primary cultures of embryonic spinal cord MNs (SMNs) (100,000 cells/well), using the TRIsure Isolation Reagent (BioLine). Ensuing treatment with the RNase-free DNase set (Invitrogen), following the manufacturer recommendations, was performed to minimize DNA impurities. The concentration and purity of RNA samples were determined by spectrophotometry at 260 and 280 nm. Retrotranscription was done using random hexamers, 500 ng of total RNA as a template and iScript^{TM} cDNA Synthesis Kit (Bio-Rad). For real time RT-PCR, each specific gene product was amplified with the MiniOpticon^{TM} System (BIO-RAD) using iTaq^{TM} Universal SYBR Green Supermix (Bio-Rad). The cDNA levels for the different samples were determined using the $2^{-\Delta\Delta Ct}$ method, being *gapdh* the housekeeping gene. The PCR primers sequences were as follows: for *atx*, forward 5′-CAGGTATGTCTTGAGGGTCAGAA-3′, reverse 5′-CCACTACTACAGCATCATCACCA-3′; for *gapdh*, forward 5′-AGAACATCATCCCTGCATCCA-3′, reverse 5′-AGATCCACGACGGACACATTG-3′. All analyses were performed in triplicate, with each experiment repeated at least twice.

2.3 | Primary cultures of SMNs

Primary cultures of SMNs were prepared from the spinal cord of mouse embryos at 12.5 days of gestation (E12.5) following an established protocol [8,21,22]. Briefly, dissected ventral cords were first chemically (0.025% trypsin in glucose-HEPES buffer solution supplemented with 20 i.u. ml^{-1} penicillin and 20 mg ml^{-1} streptomycin) and mechanically dissociated to be subsequently collected under a 4% bovine serum albumin cushion. Centrifugation (10 min, 520 × g) on an Iodixanol density gradient (OptiPrep, Axis-Shield, Oslo, Norway) allowed to isolate the largest cells, which were once more centrifuged through a bovine serum albumin cushion. Isolated cells were pooled in a tube containing culture medium and plated at various densities depending on the type of experiment. Cultured SMNs were clearly identified by SMI32 immunofluorescence or by morphological criteria [8,21] (Figure S1). SMNs were cultured in a Neurobasal medium (Gibco, Invitrogen, Paisley, UK) supplemented with B27 (Gibco; Invitrogen), horse serum (2% v/v), L-glutamine (0.5 mM) and 2-mercaptoethanol (25 μM; Sigma-Aldrich) and a cocktail of neurotrophic factors (NTFs): 1 ng ml^{-1} brain-derived neurotrophic factor, 10 ng ml^{-1} glial cell line-derived neurotrophic factor, 10 ng ml^{-1} ciliary neurotrophic factor and 10 ng ml^{-1} hepatocyte growth factor (PreProtech, London, UK). Isolated SMNs were plated in four well

tissue culture dishes (Nunc, Thermo Fisher Scientific, Roskilde, Denmark).

2.4 | Immunohistochemistry

As previously described [8,21,22], animals, under deep anaesthesia (7% chloral hydrate), were intraventricularly injected with heparin and immediately perfused transcardially with phosphate-buffered saline (PBS) followed by 4% paraformaldehyde (PFA) in 0.1 M phosphate buffer (PB), pH 7.4, at 4°C. Lumbar spinal cords (L3–L5) were rapidly dissected and post-fixed for 2 h in 4% PFA. Specimens were cryoprotected by immersion in 30% sucrose in 0.1 M PB (4°C, overnight). Serial coronal sections (30-μm thick), obtained by means of a cryostat, were kept at −20°C in a cryoprotectant solution (glycerol/PBS, 1:1 v/v) until processing.

For immunolabelling, after PBS washing, sections were immersed in a blocking solution [2.5% (w/v) bovine serum albumin, 0.25% (w/v) sodium azide and 0.3% (v/v) Triton X-100 in PBS] for 30 min, followed by incubation (4°C, overnight) with the polyclonal primary antibodies against LPA_1 (1:200; Santa Cruz Biotechnology, Cat# sc-22207, RRID:AB_2135260) developed in goat and/or SMI32 (1:8,000; Covance Research Products Inc., Cat# SMI-32R-500, RRID:AB_509998) developed in mouse. Next, the tissue was rinsed with PBS and incubated for 1 h at room temperature with Cy3- and Cy5-conjugated anti-mouse and/or anti-goat IgGs or biotinylated anti-mouse IgG (1:250; Jackson ImmunoResearch Laboratories) as secondary antibodies. Sections for immunofluorescence were washed with PBS and mounted on slides with a solution containing propyl gallate (0.1 mM in PBS/glycerol, 1:9 v/v). Sections were analysed using an Olympus FV1000-MPE confocal microscope for fluorescence microscopy (Olympus, Japan). Images were acquired through a z-plane in which maximum antibody penetration was evidenced. The pinhole opening was 1 Airy unit. For comparison between different experimental conditions, the acquisition setting was kept identical. Animals and tissue were processed in parallel. Since these experiments were performed in parallel with others aimed to evaluate the effects of LPA_1 inhibition, vehicle-treated animals were the same as in our previous report [22]. LPA_1-immunoreactivity in the ventral horn was examined following analytical methods recently described [24]. Briefly, images were processed for background subtraction to obtain the maximum dynamic range of greyscale (from 0 to 250) and analysed using the software provided by Olympus. In all cases, the area delimiting the ventral horn of the lumbar spinal cord was manually traced, and for each region, the mean and integrated fluorescence intensity was measured. For a more detailed inspection of LPA_1-immunoreactive patches, images for quantification were flattened and background-filtered to enhance cluster outlines and a user-defined intensity threshold was applied to select patches as previously described [22,24,25]. To delineate LPA_1-immunoreactive structures, images were subjected to a smoothing filter (same for all) and subsequently were binarized based on local differences in intensity. Only patches reporting an area of $>0.04\ \mu m^2$ were taken as specific. To determine the proportion of patches that co-localize with SMI32-positive structures, a grid composed of 16 squares (10 μm × 10 μm) was distributed along with the ventral horn, and then, eight randomly selected squares were analysed in each section. Regions of interest were acquired in sections obtained from at least three animals per condition.

For MNs quantification in the L3–L5 segments, biotin was detected by means of the avidin–biotin–peroxidase system (Pierce, Rockford, IL, USA) using as chromogen 3,3-diaminobenzidine tetrahydrochloride. Sections were mounted on slides, dehydrated, covered with DePeX and visualized under light microscopy using an Olympus IX81 inverted microscope. The number of neurons with a well-defined nucleus was quantified in one of each three serial sections through the L3–L5 segments of the lumbar spinal cord. SMI32-identified MNs were counted in 30 coronal sections of the lumbar spinal cord from 4-month-old mice. All quantifications were carried out by researchers blinded to the treatment groups. In all cases, omission of the primary antibodies resulted in no detectable staining.

2.5 | Assessment of phenotypic disease advance in SOD1-G93A mice

These procedures were performed as previously described [8,22]. Briefly, transgenic males were received at the pre-symptomatic stage (P30). Then, habituation sessions for rotarod and grip strength began at P45. One or two valid measures were obtained before drug administration beginning at P60. Behavioural studies were carried out by researchers blinded for treatments. Animals receiving vehicles were the same that were used in our previous work [22] since both groups of experiments were performed in parallel.

The body weight for each mouse was weekly recorded. Individual weights were normalized taking the mean value of initial measures as 100%. At the beginning of the study, mean body weight was similar for the different cohorts used in each experimental series (8th week: vehicle: 25.8 ± 0.4 g, PF-8380: 25.1 ± 0.4 g, $p = 0.218$, Student t-test). Survival was analysed by means of Kaplan–Meier survival analysis with log-rank tests for statistical significance. The end-stage was defined as the day when mice were unable to right themselves 30 s after being placed on aside. At this time point, animals were euthanized using a carbon dioxide-enriched atmosphere.

Evaluation of motor function was assessed by rotarod, runtime and grip strength tests. *Rotarod* test was carried out to judge motor coordination, strength and balance. Animals were daily trained for 1 week before data acquisition. Mice were placed individually on a cylinder (3.4 cm in diameter), rotating at a constant speed of 15 rpm. The longest latency without falling for each animal was recorded once per week, after three attempts to keep onto the rotarod (Rotarod LE8500, Panlab SA, Barcelona, Spain). The cut-off time was taken at 180 s. In each experimental series, only mice that spent at least 180 s in rotarod before beginning drug administration were included in the study. *Runtime* was the time required by the mice to run along a track of 50 cm length and was weekly determined. Muscle strength of forelimbs was monitored on a *grip strength* meter (Grip Strength Meter, BIOSEB, Chaville, France) twice a week for each mouse. The animal apprehended by the tail, once confirmed that its forelimbs were gripping a T-bar, was pulled upwards at a 60° angle. The T-bar was coupled to a force transducer and grip strength was measured in grams. The highest outcome of three trials per mouse was recorded for each session. The mean value/week for each mouse was taken to construct the time course of grip strength for the different cohorts.

2.6 | Oligonucleotides administration, drugs, and treatments

A small-interfering RNA directed against mRNA for lpa_1 (siRNA$_{lpa1}$) and a non-targeting siRNA (cRNA), taken as control, was administered as previously described [22]. The target sequence for the siRNA$_{lpa1}$ was 5′-UCAUUGUGCUUGGUGCCUU-3′ the same as in our previous report [21]. This oligonucleotide robustly reduced mRNA$_{lpa1}$ levels but did not affect the other isoreceptors (mRNA$_{lpa2-6}$) [21]. Briefly, neonatal rat pups (P5) received a single injection of oligonucleotides [21,22]. Anaesthetized animals (as above) were placed in a stereotaxic instrument (David Kopf Instruments, Tujunga, CA). siRNA$_{lpa1}$ or cRNA (2 μg per rat; Accell, Dharmacon Inc., Lafayette, CO) dissolved in 2 μl of RNase-free PBS was injected at a rate of 0.5 μl min^{-1} by means of a microsyringe (5 μl, Hamilton Company, Tokyo, Japan). The needle end was visually guided by means of a surgical microscope to deliver oligonucleotides into the fourth ventricle. After the injection, the needle was left in place for 5 min, then slowly removed. Subsequently, the incision was sutured, cleaned with an aseptic solution (povidone-iodine) and the animals were allowed to survive 2–4 days for electrophysiological recordings. All animals received a post-operative injection of penicillin (20,000 i.u. kg^{-1}; i.m.) in order to prevent infection. Pirazolone (0.1 mg kg^{-1}; i.m.) was given on awakening for post-operative analgesia.

As previously described [22], for patch-clamp recordings, brainstem slices, at the level of the HN, were initially perfused for 10 min with normal aCSF to obtain baseline control data (Before condition). Next, slices were superfused for 10–15 min with aCSF supplemented with PF-8380 (1 μM) before voltage responses were acquired again. Finally, a last round of acquisition was taken after a 10 min washout with drug-free aCSF. Since electrophysiological effects of the drug on HMNs were all reversed to before-like values, these data have been omitted for clarity.

For treatment with PF-8380 (Sigma-Aldrich, St. Louis, USA) of adult mice, the drug was dissolved in sterilized drinking water supplemented with sucrose (1%). Each animal received daily 5 ml of the drug/vehicle solution to ensure that each mouse received the appropriate dosage (1 mg kg^{-1} d^{-1}). Vehicle (1% sucrose) and PF-8380 containing solutions were freshly prepared each 3 days. Treatments began at 2 months of age.

2.7 | Statistical analysis

Summary data are all presented as mean ± SEM. The number of analysed specimens per experimental paradigm, and statistical tests applied to each data set are indicated in figure legends or in Section 3. Statistical analysis was performed using SigmaPlot (Systat Software, Inc.). The minimum significance level was set at $p < 0.05$. Statistical tests were employed for all data sets with similar variance. For comparison between two groups, normally distributed data were analysed by unpaired or paired Student *t*-test, unless otherwise stated, while non-parametric data sets were assessed by Mann–Whitney *U*-test. One-way or two-way ANOVA followed by *post hoc* Holm-Sidak method was employed for comparison of three or more groups that passed the normality test. No data points were excluded from the statistical analysis unless otherwise noted.

3 | RESULTS

3.1 | PF-8380 reduces HMN IME via LPA$_1$

Since baseline LPA$_1$-mediated signalling maintains HMN IME in the brainstem slice preparation [22], it is highly probable that endogenous activity of the major LPA-synthesizing enzyme ATX also impacts HMN IME in this experimental condition. Thus, we first tested whether the ATX inhibitor PF-8380 [26] affects HMN IME in coronal slices obtained from rat pups (P5–P9). Whole-cell patch-clamp recordings of HMNs showed that the addition of the ATX inhibitor (1 μM for 10 min) to the bath solution produced a strong hyperpolarization (−11.2 ± 3.6 mV) of the membrane (Figure 1A,B; Table 1). This alteration was accompanied by an increase
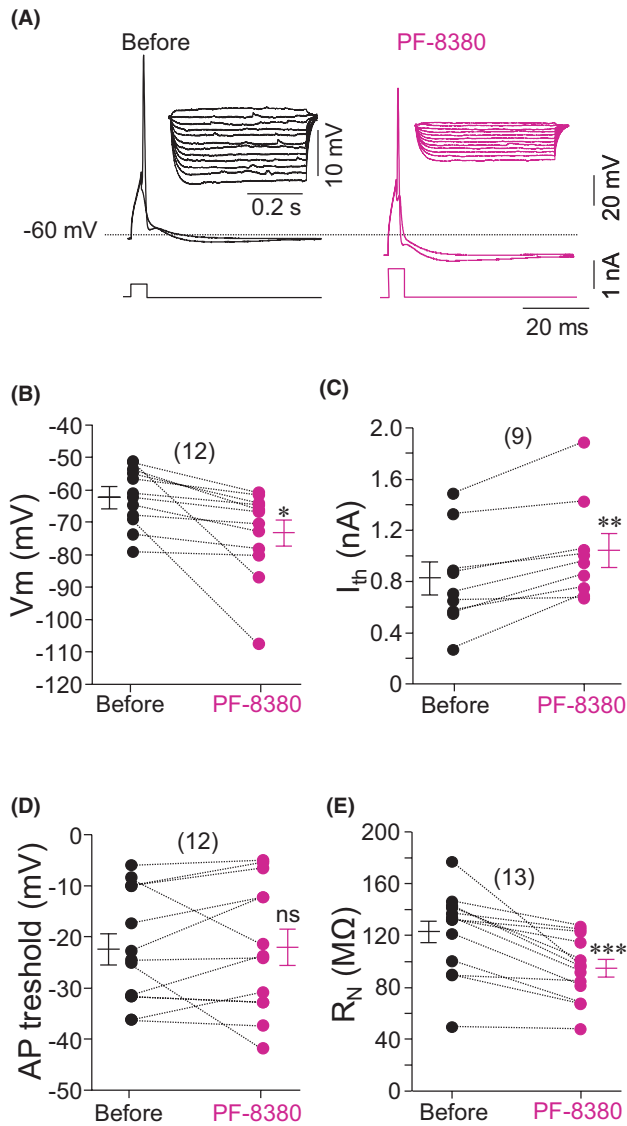
(A)

FIGURE 1 PF-8380 affects the intrinsic membrane properties of HMNs. (A) Superimposed graded (AP failure) and AP voltage responses to depolarizing current pulses delivered at threshold intensities were recorded in a HMN from a P7 rat before and following 10 min exposure to PF-8380 (1 μM). The currents required to reach the threshold for AP generation (I_{th}) in each condition are shown at the bottom of the traces. Insets, voltage responses to step hyper-polarizing currents applied to determine R_N in each condition. (B–E) Vm (B), I_{th} (C), AP threshold (D) and R_N (E) data values of HMNs recorded before and after perfusion with PF-8380. The number of analysed HMNs in each group is in parentheses. Error bars, SEM. *$p < 0.05$, **$p < 0.01$, ***$p < 0.001$; ns, not significant; by paired Student t-test

(+0.2 ± 0.1 nA) in the current threshold (I_{th}) to elicit an AP. However, the AP voltage threshold (AP threshold) was unaltered (+0.4 ± 2.1 mV) by the ATX inhibitor (Figure 1A,C,D; Table 1). These outcomes indicate that the PF-8380 induced reduction of I_{th} is mainly linked to the hyperpolarization shift observed for Vm rather than to a depolarization shift in the AP threshold. Finally, PF-8380 induced an abrupt reduction (−28.4 ± 6.0 MΩ) in HMN R_N, a passive membrane property reflecting the electrical resistance of the whole surface membrane, a key determinant in the neuron's IME (Figure 1A,E; Table 1). Electrophysiological effects of PF-8380 on HMNs were all reversed after 10 min of washing and have been omitted for clarity. Therefore, PF-8380 led HMNs to a transitory hypo-excitable state, indicating that baseline activity of ATX, in our experimental conditions, contributes to maintain/modulate HMN IME.

As we previously reported [22], the ATX-synthesized lysophospholipid LPA affects HMN IME by acting on the G-protein-coupled receptor LPA_1 which, subsequently, modulates the background K^+ channel TASK1. Therefore, to reinforce the idea that baseline ATX activity controls HMN IME throughout LPA_1-mediated signalling, we tested the effects of PF-8380, as above, on HMNs from rat pups that received at P5 microinjection of $siRNA_{lpa1}$ or cRNA in the fourth ventricle. In the cRNA condition, PF-8380 induced expected Vm hyperpolarization, increase in I_{th}, and reduction in R_N, without affecting AP threshold (Figure 2; Table 2). Strikingly, alterations induced by the ATX inhibitor were fully absent in HMNs from animals treated with $siRNA_{lpa1}$ (Figure 2; Table 2). Given that this protocol efficiently knockdowns LPA_1 without affecting the expression of the other isoreceptors [21,22], these outcomes strongly support that endogenous ATX impacts HMN IME via, at least, LPA_1.

3.2 | Upregulation of $mRNA_{atx}$ levels in the spinal cord of SOD1-G93A mice

Next, to gain support for a feasible contribution of ATX in disease progression in the mouse model of ALS, qRT-PCR analysis of $mRNA_{atx}$ expression was performed in the lumbar spinal cord of SOD1-G93A mice and their non-Tg littermates at different stages of disease progression. Noticeably, transcripts were already upregulated in transgenic samples extracted from 1-month-old mice

TABLE 1 Effect of the ATX inhibitor PF-8380 on intrinsic membrane properties of HMNs

Treatment	Vm (mV)	I_{th} (nA)	AP threshold (mV)	R_N (MΩ)
Before	−62.0 ± 2.6	0.824 ± 0.1	−22.4 ± 3.0	122.9 ± 9.1
PF-8380	−73.2 ± 3.9*	1.042 ± 0.1**	−22.1 ± 3.5^{ns}	94.6 ± 6.8***

*$p < 0.05$, **$p < 0.01$, ***$p < 0.001$; ns, not significant; by paired Student t-test.

FIGURE 2 siRNA$_{lpa1}$ avoids PF-8380 effects on analysed intrinsic membrane properties of HMNs. As in Figure 1, but recordings were performed in HMNs obtained from rat pups that received at P5 a single injection of cRNA or siRNA$_{lpa1}$ into the fourth ventricle. V_m (B), I_{th} (C), AP threshold (D) and R_N (E) data values of HMNs were recorded before and after perfusion with PF-8380 receiving the stated oligonucleotides. The number of analysed HMNs in each group is in parentheses. Error bars, SEM. *$p < 0.05$, **$p < 0.01$, ***$p < 0.001$; ns, not significant; by paired Student t-test
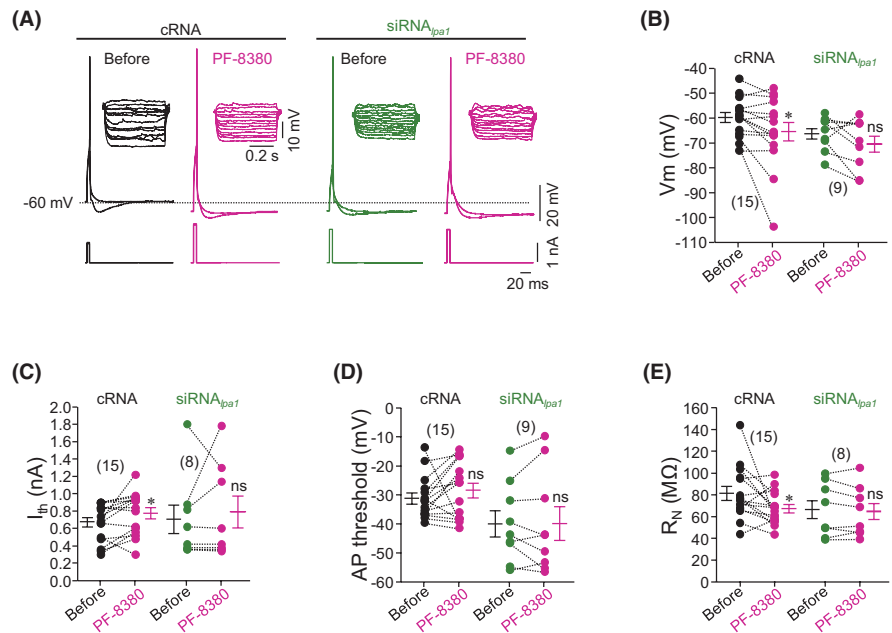

TABLE 2 Effect of the ATX inhibitor PF-8380 on intrinsic membrane properties of HMNs from rat pups receiving a single injection of the indicated oligonucleotides at P5

Treatment	V_m (mV)	I_{th} (nA)	AP threshold (mV)	R_N (MΩ)
cRNA				
Before	-59.8 ± 2.0	0.661 ± 0.1	-31.3 ± 1.9	81.3 ± 6.4
PF-8380	-65.5 ± 3.7*	0.773 ± 0.1*	-28.5 ± 2.5^{ns}	67.2 ± 3.9*
siRNA$_{lpa1}$				
Before	-66.4 ± 2.3	0.705 ± 0.2	-40.0 ± 4.5	66.2 ± 8.8
PF-8380	-70.6 ± 3.4^{ns}	0.790 ± 0.2^{ns}	-39.9 ± 5.8^{ns}	64.7 ± 8.2^{ns}

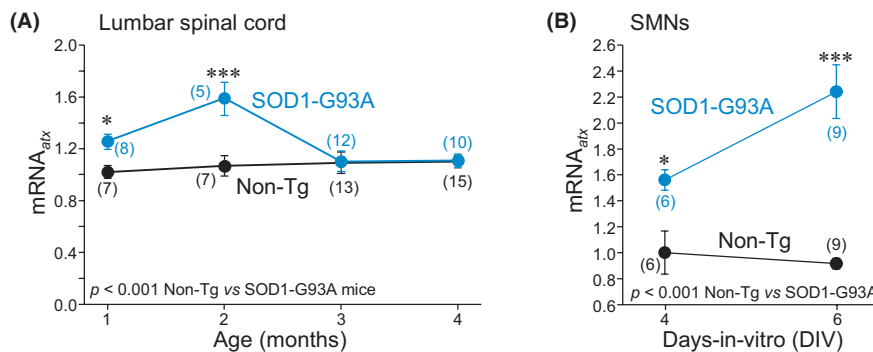*$p < 0.05$, ns, not significant; by paired Student t-test.

FIGURE 3 Changes in the expression levels of mRNA$_{atx}$ in the spinal cord of ALS mice and in SMNs from SOD1-G93A embryos. (A) Time course of changes in mRNA$_{atx}$ expression in the spinal cord of SOD1-G93A mice and their non-Tg littermates. Values were normalized taking the mean value for 1-month-old non-Tg mice as 1. (B) mRNA$_{atx}$ expression at the indicated days-in-vitro, determined by qRT-PCR, in SMNs isolated from non-Tg and SOD1-G93A embryos. $gapdh$ was the housekeeping gene. mRNA$_{atx}$ values were normalized relative to the mean value obtained at 4 DIV for non-Tg SMNs. The number of mice (A) or SMNs extractions (B) in each group is in parentheses. Error bars, SEM. *$p < 0.05$, **$p < 0.01$, ***$p < 0.001$; by two-way ANOVA with *post hoc* Holm-Sidak method. Statistic outputs between genotypes are displayed in plots

(SOD1-G93A: $126.0 \pm 5.8\%$, non-Tg: $102.1 \pm 5.0\%$), the first time point tested (Figure 3A). mRNA$_{atx}$ levels rose in 2-month-old animals (SOD1-G93A: $159.2 \pm 13.0\%$, non-Tg: $106.8 \pm 7.8\%$) and declined to non-Tg-like levels in 3-month-old (SOD1-G93A: $110.2 \pm 7.9\%$,

non-Tg: $109.1 \pm 8.2\%$) and 4-month-old (SOD1-G93A: $111.0 \pm 4.9\%$, non-Tg: $110.0 \pm 4.7\%$) ALS mice (Figure 3A). Thus, the increase of mRNA$_{atx}$ expression in the spinal cord of SOD1-G93A mice occurs at pre-symptomatic (1–2-month-old) stages, therefore preceding MN loss, but

dropped to a control-like condition at early symptomatic (3-month-old) and symptomatic phases (4-month-old) (Figure 3A), when MN loss is already evident. At this point, it is interesting to remark that the increase in mRNA$_{atx}$ levels also occurred prior to the enhancement of mRNA$_{lpa1}$ observed in these mice [22]. This supports a gain in the ATX-LPA$_1$ signalling axis that precedes MN loss in ALS mice.

To explore the possibility that MNs were feasible sources for mRNA$_{atx}$ enhancement, and given that ATX is an ectoenzyme, we measured and compared transcript levels in primary cultures of SMNs isolated from SOD1-G93A and non-Tg mouse embryos at two different differentiation days *in vitro* (4 DIV and 6 DIV). These time points were selected based on our preceding report, which shows that in SMNs isolated from SOD1-G93A mice the expression levels of mRNA$_{lpa1}$ are normal at 4 DIV and abruptly increase at 6 DIV relative to non-Tg-cultured cells [22]. Interestingly, mRNA$_{atx}$ levels were significantly higher in SMNs isolated from SOD1-G93A (156.1 ± 7.7%) than in those extracted from non-Tg (100.0 ± 16.6%) embryos at 4 DIV (Figure 3B). The difference was even more pronounced (non-Tg: 91.6 ± 3.9%, SOD1-G93A: 224.2 ± 20.5%) at 6 DIV (Figure 3B). Altogether, the outcomes indicate that alterations in mRNA$_{atx}$ levels precede changes in mRNA$_{lpa1}$ expression both, in the lumbar spinal cord of SOD1-G93A mice and in SMNs extracted from transgenic embryos during the differentiation progress [22]. Furthermore, it can be suggested that MNs could be a feasible origin for mRNA$_{atx}$ upregulation observed in ALS mice.

3.3 | PF-8380 delays MN loss in the ALS SOD1-G93A model

The increase of LPC, the main ATX substrate, in the ventral horn of ALS patients [16], together with mRNA$_{atx}$ over-expression in the spinal cord of SOD1-G93A mice, highlights ATX as a pivotal partner in the pathogenesis of disease and as a target for further pre-clinical assessment. To explore this issue, we examined the potential neuroprotective effect of chronic *in vivo* treatment with the orally bioavailable ATX inhibitor PF-8380 in the SOD1-G93A mouse model. In this murine line, disease progression predominantly courses from hind to forelimbs. Therefore, we focused our *in vivo* treatment studies on MN survival in the motor pools located at the lumbar spinal cord. Feasible neuroprotection against MN degeneration was analysed by quantifying the number of SMI32-positive MNs in the L3–L5 lumbar segment from 4-month-old mice [8,22]. Chronic administration of PF-8380 (1 mg kg^{-1} d^{-1}) in the drinking water beginning at 2 months of age exerted beneficial effects on MNs in the ALS model. Under PF-8380 treatment, the number of MNs present in the lumbar spinal cord of SOD1-G93A mice was higher (+29.2 ± 11.5%) than in age-matched transgenic animals treated with vehicle (Figure 4). This finding indicates that treatment with the ATX inhibitor delays loss of lumbar MNs in the ALS model.

3.4 | Benefits of PF-8380 on phenotypic disease progression in SOD1-G93A mice

We subsequently evaluated whether the neuroprotective effect of PF-8380 on SOD1-G93A MNs translates into a change in the phenotypic progression of the disease. For that purpose, forelimb grip strength, latency to fall from a rolling cylinder (Rotarod), time to cover a distance of 50 cm (Runtime), time for symptom onset, the evolution of body weight and survival time were analysed in the vehicle and PF-8380 treated groups of SOD1-G93A mice (Figure 5). As a starting point to construct the cumulative probability curve of symptom onset, we used the first day in which a mouse showed motor function
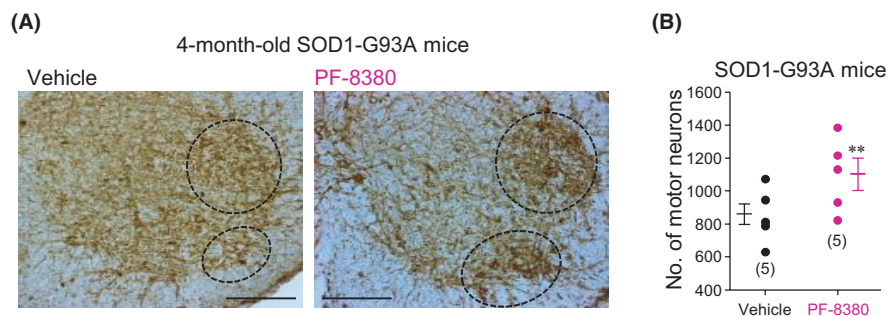

(A) 4-month-old SOD1-G93A mice

Vehicle   PF-8380

(B) SOD1-G93A mice

No. of motor neurons

FIGURE 4 Treatment with PF-8380 delays MN loss in ALS mice. (A) Representative microphotographs of lumbar spinal cord sections immunostained for SMI32 from 4-month-old SOD1-G93A mice that received vehicle or PF-8380 (1 mg kg^{-1} d^{-1}) in the drinking water beginning at P60. Boxed areas indicate SMI32-positive MN pools. Scale bar: 65 μm. (B) Quantification of the number of SMI32-identified MNs in the L3–L5 spinal cord segments for each condition. Since these experiments were performed in parallel with others intended to evaluate the effects of the administration of the LPA$_1$ inhibitor AM095 [22], the vehicle group is the same for both assays. The number of analysed mice in each group is in parentheses. Error bars, SEM. *$p < 0.05$, **$p < 0.01$, ***$p < 0.001$; ns, not significant; by Student t-test
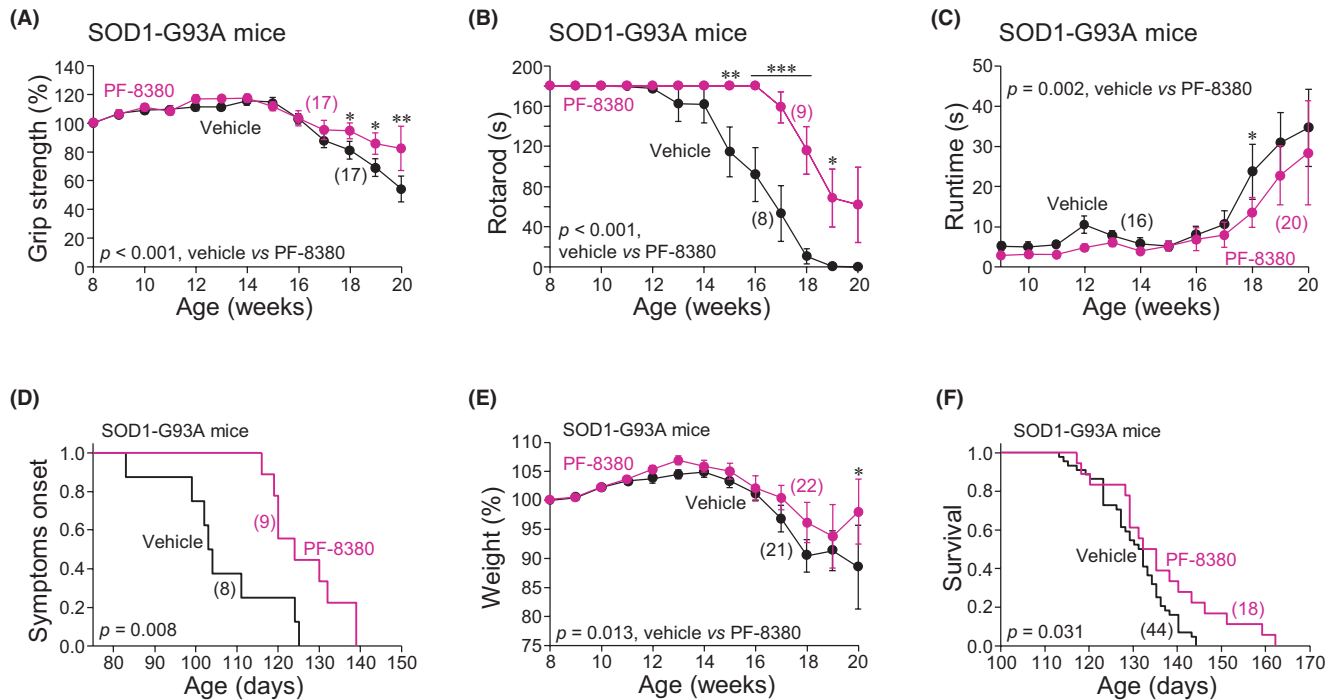
FIGURE 5 Neuroprotective effects of PF-8380 in the SOD1-G93A mouse model of ALS. (A) Time course of forelimb grip strength (in per ent) decline in vehicle- and PF-8380-treated SOD1-G93A mice. Strength measured at 9 weeks of age/mouse was taken as 100%. (B) Age-related changes in rotarod performance for both treatment groups. Rotarod test was performed to evaluate the time course of deficits in motor coordination, strength and balance as well as to construct the cumulative probability curve of symptoms onset in (D). (C) PF-8380 delayed runtime (time animals took to run a track of 50 cm) decline compared with vehicle. (D–F) Cumulative probability curves of symptom onset (D), the time course of mean body weight (E) and survival (F) for vehicle- and PF-8380-treated SOD1-G93A mice. The number of mice in each group is in parentheses. The vehicle groups are the same as those in Gento-Caro and colleagues [22]. Error bars, SEM. *$p < 0.05$, **$p < 0.01$, ***$p < 0.001$; n.s., not significant; by two-way ANOVA with *post hoc* Holm-Sidak method (A–C, E). Log-rank test, Kaplan–Meier analysis was applied to (D and F). Statistic outputs comparing both treatments are displayed in plots

deficits on the rotarod test (≥10% reduction in the time to fall) followed by progressive performance deterioration in the next sessions [22]. Noticeably, the PF-8380-treated group displayed better outputs in these tests in comparison with the vehicle-treated SOD1-G93A cohort (Figure 5). For example, taken 18-week-old point for comparison, PF-8380 significantly improved grip strength (+16.3 ± 6.7%), time in rotarod (+105.1 ± 23.8 s) and runtime (−10.2 ± 3.7 s) in comparison to outputs displayed by vehicle-receiving ALS mice (Figure 5A–C). In addition, PF-8380 delayed substantially symptom onset (+20.2 ± 2.9 days, difference between mean values), improved weight loss advancement and prolonged lifespan (+5.6 ± 3.0 days, difference between mean values) in SOD1-G93A mice (Figure 5D,E). In studies parallel to those presented herein, analysis of transgene expression in a random sampling of several SOD1-G93A cohorts subjected to diverse treatments did not show, in any case, differences in the levels of SOD1-G93A transcripts [8,22]. It is therefore improbable that positive effects observed here can be as a result of different expression levels of the human SOD1-G93A in both cohorts. These findings support a critical role of ATX in the pathophysiology of this lethal neurodegenerative disease providing also

preclinical validation of ATX knockdown and/or function inhibition as a potential therapeutic strategy in ALS.

Whether higher doses of PF-8380 may lead to further improvement in disease progression in this transgenic mouse model of ALS merits further investigation. In conclusion, these outcomes point to ATX inhibitors as potential pharmacological candidates to be tested in translational clinical assays in ALS.

3.5 | PF-8380 reduces LPA$_1$ expression in SOD1-G93A MNs

It is interesting to remark at this point that LPA$_1$ is upregulated in the ventral horn and in MNs at the lumbar spinal cord of this ALS model [22]. When comparing the time course of mRNA$_{atx}$ and mRNA$_{lpa1}$ expression in ALS mice, it becomes apparent that mRNA$_{atx}$ over-expression precedes mRNA$_{lpa1}$ upregulation in the lumbar spinal cord of SOD1-G93A mice (Figure 6A). Strikingly, rising levels of LPA following its intrathecal administration leads to LPA$_1$-dependent LPA$_1$ upregulation in dorsal root ganglions [27]. In addition, two different strategies, both leading to LPA$_1$ knockdown in MNs,
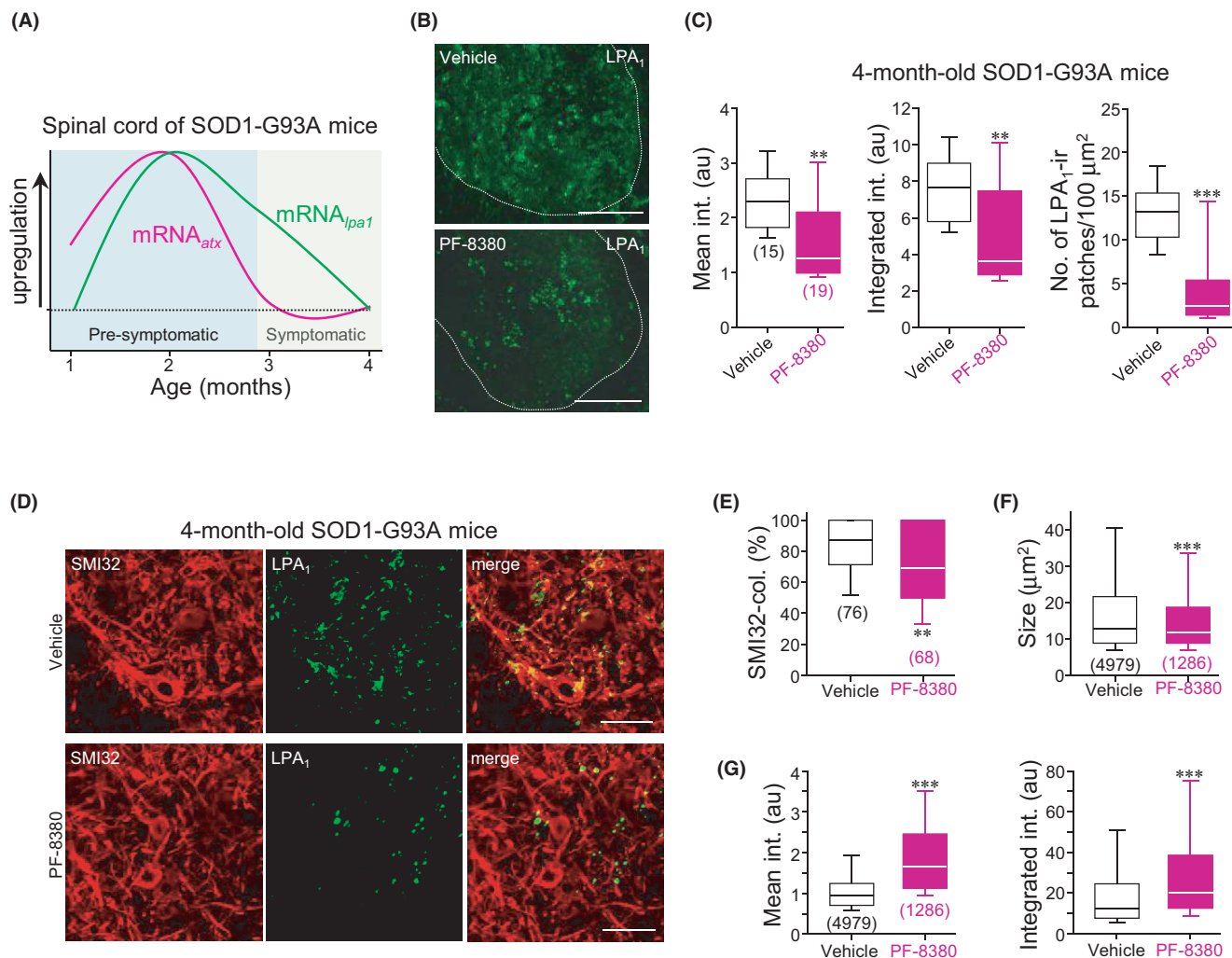
FIGURE 6 PF-8380-treatment alters LPA$_1$-immunoreactivity in the ventral horn of SOD1-G93A mice. (A) Schematic plot modelling the time course of changes in the expression of mRNA$_{atx}$ (from data in Figure 2A) and mRNA$_{lpa1}$ (from data in Figure 5B in [22]) in the lumbar spinal cord of SOD1-G93A mice. Note that upregulation of mRNA$_{atx}$ precedes increase in the levels of mRNA$_{lpa1}$. Decline of mRNA$_{atx}$ to non-Tg-like levels (horizontal dotted line) also occurred before mRNA$_{lpa1}$ drop. (B) Low magnification confocal images of immunolabelling for LPA$_1$ in the ventral horn of 4-month-old SOD1-G93A mice receiving the indicated treatments. Dotted lines delimit ventral horn and the area for quantitative analysis. (C) Box-plots of the mean (left), integrated (middle) intensity (int.) (in arbitrary units, a.u.) and number of LPA$_1$-immunoreactive (LPA$_1$-ir) patches/100 μm^2 (right) in the ventral horn of SOD1-G93A receiving vehicle or PF-8380. (D) High-magnification confocal images of ventral horns double immunolabelled for LPA$_1$ (green) and the MN marker SMI32 (red). (E–G) Characterization of LPA$_1$-ir patches in the ventral horn of mice expressing the indicated genotypes. Box-plots of the number of patches co-localizing with SMI32-ir structures (SMI32-col., in percent, E), the mean size (in μm^2, F) and mean and integrated fluorescence intensity (in a.u., G). Scale bars: (B) 200 μm; (D) 50 μm. Number of analysed specimens in each group is in parentheses. Box-plots show median (white line) and the 25–75% range as box, the whiskers indicate 5–95% range. *$p < 0.05$, **$p < 0.01$, ***$p < 0.001$; ns, not significant; by Student t-test (E–G) or non-parametric Mann–Whitney U-test (C)

were neuroprotective in the ALS mouse model [22]. These findings led us to hypothesize that the mechanism of action by which chronic treatment with PF-8380 slows down disease progression in SOD1-G93A mice might, at least in part, involve LPA$_1$ knockdown in the ventral horn and in MNs.

To assess this possibility, double immunolabelling for LPA$_1$ and the MN marker SMI32 was performed in the ventral horn of the lumbar spinal cord from 4-month-old transgenic animals receiving chronic treatment with vehicle or PF-8380. Strikingly, the ATX inhibitor led to a strong reduction in LPA$_1$ expression in the ventral horn

of treated animals (Figure 6B,C; Table 3). The density (number/100 μm^2) of LPA$_1$-immunoreactive patches, probably indicating clusters of the receptor, was drastically reduced ($-65.2 \pm 9.6\%$) in PF-8380-treated animals relative to the control group (Figure 6C, Table 3). It was interesting to observe that LPA$_1$-positive patches co-localizing with SMI32-immunoreactive structures, and therefore likely belonging to MNs, were proportionally more affected by PF-8380 than those that did not co-localize with the MN marker (vehicle, $82.0 \pm 2.7\%$; PF-8380, $67.8 \pm 3.5\%$ of patches co-localizing with SMI32-immunoreactive structures) (Figure 6D,E;

TABLE 3 Characterization of LPA$_1$-immunoreactive patches in the ventral horn of the lumbar spinal cord from 4-month-old SOD1-G93A mice

Treatment	Number/100 μm^2	Co-localizing with SMI32 (%)	Size (μm^2)	Mean intensity	Integrated intensity
Vehicle	13.5 ± 1.2	82.0 ± 2.7	21.1 ± 0.4	1.2 ± 0.01	25.7 ± 0.8
PF-8380	4.7 ± 1.3[#]	67.8 ± 3.5*	17.5 ± 0.5*	1.9 ± 0.03*	37.4 ± 1.5*

Note: Vehicle condition is the same that in Gento-Caro et al. [22], since these experiments were performed in parallel with those previously reported for the LPA$_1$ inhibitor AM095. [#],*$p < 0.001$, by Student t-test (*) or non-parametric Mann–Whitney U test ([#]).

Table 3). Furthermore, the mean size of the remaining LPA$_1$-positive patches was smaller (−17.1 ± 2.4%) in the group treated with the ATX inhibitor than in vehicle-treated animals, even though they exhibited relatively higher fluorescence intensity in the former of these conditions (Figure 6F,G; Table 3). These outcomes suggest, either or both of these possibilities, that PF-8380 mainly affected larger patches with lower receptor densities and/or that it induced a rearrangement of LPA$_1$ receptors.

4 | DISCUSSION

The major LPA-synthesizing ectoenzyme ATX has been identified as a protein whose endogenous activity regulates MN excitability, at least, through LPA$_1$. Several proteins, pivotal in the control of MN IME, have been shown to undergo dysregulation in this cell type preceding MN death in the SOD1-G93A mouse model of ALS. Interfering with most of these factors was a suitable strategy to delay disease advance in ALS mice [8,22]. Within this framework, proofs contributed here also point to ATX dysregulation as a pathogenic event previous to MN loss in transgenic animals. Further, an ATX inhibitor was neuroprotective in ALS mice by a mechanism of action that, at least in part, engages downregulation of LPA$_1$ expression in MNs. Thus, ATX is proposed as a potential target and/or biomarker in ALS, and ATX inhibitors are highlighted as reasonable tools for therapeutic use in this lethal pathology.
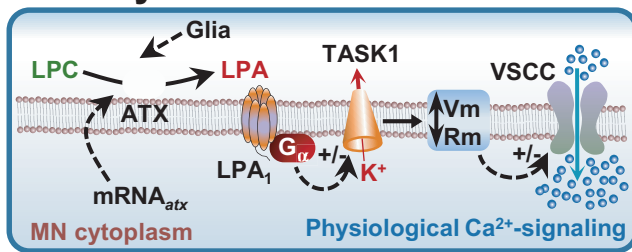
Intrinsic membrane properties and excitation/inhibition (E/I) balance determine neuronal and network excitability. Excitability alterations are considered to lie behind the vulnerability of various neuronal subtypes whose loss is causative in the development of neurodegenerative disorders including ALS [1,3,8,28,29]. Of relevance in this respect, ATX inhibition rescued schizophrenia-related hyper-excitability syndromes in mouse models for psychiatric disorders influencing glutamatergic neurotransmission, then raising the proposal that ATX inhibition is a general method to reverse cortical excitability by impacting E/I balance [30]. However, no findings so far have suggested a role of ATX inhibition in regulating excitability by directly impacting neuronal intrinsic membrane properties. Here, we state that baseline ATX activity also affects excitability by regulating neuronal IME acting, at least, through the G-protein-coupled receptor LPA$_1$. Thus, PF-8380 altered

Vm, membrane resistance, and current threshold for AP generation in MNs, but it did not disturb the voltage threshold for spike initiation. All these changes were absent after the LPA$_1$ knockdown. The majority of ATX-mediated biological activities are associated with its main product LPA by acting on a family of six cognate G-protein-coupled receptors [15]. Baseline LPA–LPA$_1$ signalling also modulates intrinsic membrane parameters of MNs [22] in the same direction and at the same degree as endogenous ATX activity. Hence, we propose that the ATX–LPA–LPA$_1$ axis controls MN excitability by, at least in part, modulating TASK1 'leak' potassium channels (Figure 7) [22].

ATX is widely expressed throughout body tissues, with the highest mRNA levels detected in the brain and spinal cord among other organs. ATX is secreted as an active lysophospholipase D that acts locally rather than systemically, by its binding to cell surface integrins [31]. Thus, ATX-mediated local synthesis of extracellular LPA can bind to LPA$_1$ at the MN leading to inhibition of TASK1 channels which in turn can promote excitotoxic MN degeneration (Figure 7) [22]. In support, diverse strategies that promoted TASK1 functional expression in MNs had, like the ATX inhibitor in the present work and interfering with LPA$_1$ signalling [22], a neuroprotective effect in the SOD1-G93A model [8]. The expression pattern of the different partners foresees that signalling through ATX–LPA$_1$–TASK1 axis affects many neuronal subpopulations vulnerable to certain neuropathological conditions (http://mouse.brain-map.org/) [32]. In this regard, dysregulation of ATX–LPA$_1$ signalling may contribute to a wide variety of CNS and PNS disorders such as neuropathic pain, schizophrenia, multiple sclerosis, Alzheimer's disease, traumatic brain injury, major depressive disorder, HIV-induced brain injury and peripheral nerve injury [15], among others. Furthermore, the possibility that ATX–LPA$_1$ axis impacts MN excitability by modulating E/I balance cannot be discarded since LPA–LPA$_1$ signalling differentially affects glutamatergic and GABAergic inputs on MNs [21]. In summary, the ATX–LPA$_1$ axis might determine neuronal and network excitability by impacting on both, E/I balance in neural circuits and intrinsic membrane electrical properties of neurons.

Disruption of LPA signalling has been associated with multiple disease processes [15]. The importance of the metabolic pathway for LPA synthesis via ATX is illustrated by the half-normal plasma LPA levels found in
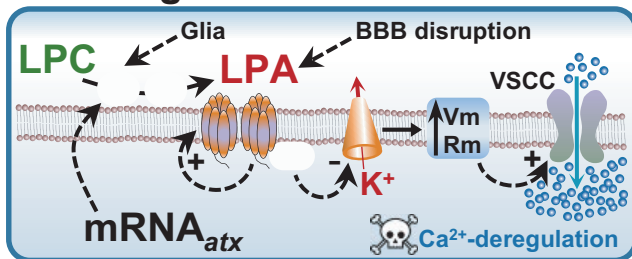
FIGURE 7 Schematic modelling of the role of ATX-LPA-LPA$_1$ signalling in degeneration of MNs in the SOD1-G93A mouse model. At physiological conditions (top), extracellular ATX, either from MN and/or glial (http://mouse.brain-map.org/) origin, synthesizes LPA taking LPC as the main substrate. LPA, via de G-protein-coupled receptor LPA$_1$, modulates the activity of the background K$^+$ channel TASK1, which determines MN IME and subsequently alters the open probability of voltage-sensitive Ca^{2+} channels (VSCCs) [22]. At this condition, a controlled influx of Ca^{2+} through these channels mediates intracellular physiological signalling. At pathological conditions, such as those implicated in the progression of disease in the SOD1-G93A mouse model, some lines of evidence support that ATX-LPA-LPA$_1$ over-signalling could favour excitotoxic degeneration of 'sick' MNs. mRNA$_{atx}$ upregulation from MNs and/or activated glial cells together with stimulation of production/release of the ATX substrate LPC [15] likely lead to increase LPA synthesis. The rise in LPA concentration might be potentiated by distortion of blood–brain barrier (BBB) function and integrity during disease progression [36,37]. The increase in LPA levels can induce LPA$_1$-dependent LPA$_1$ upregulation [27] in SOD1-G93A MNs. Once this scenario is established, the ensuing ATX-LPA-LPA$_1$ over-signalling can derive in the inhibition of TASK1 channels, enhancing IME which, in turn, increases the opening probability of VSCCs thereby exacerbating Ca^{2+} entry into the cell. Consequently, Ca^{2+} deregulation leads to Ca^{2+} overload that might contribute to MN neurodegeneration and, finally, to neuron death [8,22]. For more details, see the text

heterozygous ATX mice (*enpp*2$^{+/−}$) [33,34]. On the other hand, ATX is upregulated during several pathological conditions and leads to an accompanying increase in LPA [15]. Interestingly, comparing data contributed in Figure 3A of this paper and Figure 5B of our preceding one [22], it is evident that the increase in ATX levels in the lumbar spinal cord precedes LPA$_1$ upregulation in MNs in the SOD1-G93A mice (Figure 6A). Remarkably, an increase in LPA levels lies behind LPA$_1$-dependent LPA$_1$ upregulation in dorsal root ganglions [27]. Therefore, ATX upregulation observed in the lumbar spinal cord of SOD1-G93A mice can be likely associated with an

increase in LPA production which, in turn, might be responsible for delayed LPA$_1$ upregulation occurring in the spinal cord and MNs (Figure 7) [22]. Supporting this assumption, chronic administration of inhibitors of either ATX or LPA$_1$ [22], reduced LPA$_1$ expression in MNs, were neuroprotective for them and delayed phenotypic progression of disease in the transgenic mouse. Therefore, determination of the levels of distinct LPA species in the spinal cord, cerebrospinal fluid and/or blood in ALS mice is proposed for future investigation.

Inflammation is amongst the major pathogenic pathways for MN death in ALS. There is evidence that inflammatory stimuli may stimulate LPC production/release which is converted to functionally active LPA by ATX in chronic pain [15]. This process seems to rely on simultaneous stimulation of spinal neurokinin 1 and NMDA-type glutamate receptors triggering LPC-derived LPA production via extracellular ATX [35]. Therefore, given that excessive glutamatergic signalling is considered a major etiopathogenic episode in ALS, it might also contribute to ATX–LPA$_1$ over-signalling. In addition, whether over-expression of the ATX–LPA$_1$ axis forms part of the inflammatory process in the aetiopathogenesis of disease in the ALS model can be raised. In a scenario in which blood–brain barrier function and integrity are distorted at the onset of disease in ALS patients and before disease beginning in transgenic ALS mice models, LPA levels can increase in the CNS (Figure 7) [36,37]. This presumed increase in LPA levels could account for at least part of LPA$_1$ upregulation observed at pre-symptomatic stages in transgenic mice [22]. Additionally, feed-forward LPA-induced upregulation of transcription factors of the NFAT family could upregulate ATX expression and the ensuing LPA production [38]. Furthermore, ATX is upregulated by TNFα-mediated activation of NFkB, which is particularly relevant in the context of the inflammatory milieu by playing a major role in the expression of pro-inflammatory genes [38,39]. Strikingly, NFkB upregulation occurs in the course of disease progression in SOD1-G93A mice [40] and neuron-specific inhibition of NFkB signalling was neuroprotective in two mouse models of ALS [41]. In summary, over-expression of the ATX–LPA$_1$ axis in transgenic mice could result from the increase of LPA levels after blood–brain barrier deterioration and/or NFkB pathway activation at least in MNs, as part of the inflammatory process.

It is interesting to remark that an increased expression and activity of cytosolic PLA2 (cPLA2) have been detected in neurons, astrocytes and microglia in the spinal cord of both sporadic ALS patients [42] and SOD1-G93A mice [43]. Additionally, cPLA2-mediated LPC production, an ATX substrate, regulates neuroinflammation and triggers neurodegeneration [44]. On the contrary, specific reduction of cPLA2 in the brainstem and spinal cord significantly attenuated the development of the disease in the transgenic model [45]. Altogether, these evidences suggest that cPLA2 may

have an important role in the pathogenesis of ALS by making available higher quantities of the ATX substrate. Consequently, presumable over-signalling of the ATX-LPA$_1$ axis is expected in ALS mice before MN death (Figure 7).

Given that both, acute (stroke, trauma or epilepsy) and chronic neurodegenerative diseases (Alzheimer, Parkinson's and Huntington's diseases, HIV-associated dementia, multiple sclerosis and ALS) are associated with dysregulation of membrane excitability [1,3,28,29], our findings could have a broad impact on human neurological and psychiatric diseases. In addition to the ATX inhibitor GLPG1690 currently in phase III clinical studies for idiopathic pulmonary fibrosis, BBT-877, and BLD-0409, two potent ATX inhibitors, have been enrolled in phase Ⅰ clinical evaluations [46]. Therefore, we propose ATX as a potential target and/or a biomarker in ALS and highlight ATX inhibition/knockdown as an interesting strategy with therapeutic usefulness for this lethal pathology and other neurological conditions.

ACKNOWLEDGEMENTS

CONFLICT OF INTEREST

The authors declare that they have no conflict of interest.

AUTHOR CONTRIBUTIONS

Bernardo Moreno-López: conceptualized, designed the study and wrote the paper. David González-Forero: supervised electrophysiological experiments and reviewed the first draft of the paper. Ángela Gento-Caro, Esther Vilches-Herrando and Federico Portillo: performed experiments, data analysis and figures. Bernardo Moreno-López and David González-Forero: obtained the funding. All authors participated in a critical review of the manuscript.

ETHICS APPROVAL

Animals were obtained from an authorized supplier (Animal Supply Services, University of Cádiz, Cádiz, Spain). Animal care and handling followed the guidelines of the European Union Council (2010/63/EU, 86/609/UE) on the use of laboratory animals. Experimental procedures were approved by the local Animal Care and Ethics Committee (University of Cadiz, Cadiz, Spain) and the Ministry of Agriculture, Fisheries and Rural Development (Junta de Andalucía, Spain).

DATA AVAILABILITY STATEMENT

The data sets generated and/or analysed during the current study are available from the corresponding authors on reasonable request.

ORCID

David González-Forero https://orcid.org/0000-0001-5748-9546
Bernardo Moreno-López https://orcid.org/0000-0003-2897-6227

REFERENCES

1. Do-Ha D, Buskila Y, Ooi L. Impairments in motor neurons, interneurons and astrocytes contribute to hyperexcitability in ALS: underlying mechanisms and paths to therapy. Mol Neurobiol. 2018;55(2):1410–8. https://doi.org/10.1007/s12035-017-0392-y
2. Fogarty MJ. Driven to decay: excitability and synaptic abnormalities in amyotrophic lateral sclerosis. Brain Res Bull. 2018;140:318–33. https://doi.org/10.1016/j.brainresbull.2018.05.023
3. King AE, Woodhouse A, Kirkcaldie MT, Vickers JC. Excitotoxicity in ALS: overstimulation, or overreaction? Exp Neurol. 2016;275 (Pt 1):162–71. https://doi.org/10.1016/j.expneurol.2015.09.019
4. Bae JS, Simon NG, Menon P, Vucic S, Kiernan MC. The puzzling case of hyperexcitability in amyotrophic lateral sclerosis. J Clin Neurol. 2013;9(2):65–74. https://doi.org/10.3988/jcn.2013.9.2.65
5. Kanai K, Shibuya K, Sato Y, Misawa S, Nasu S, Sekiguchi Y, et al. Motor axonal excitability properties are strong predictors for survival in amyotrophic lateral sclerosis. J Neurol Neurosurg Psychiatry. 2012;83(7):734–8. https://doi.org/10.1136/jnnp-2011-301782
6. Ragagnin AMG, Shadfar S, Vidal M, Jamali MS, Atkin JD. Motor neuron susceptibility in ALS/FTD. Front Neurosci. 2019;13:532. https://doi.org/10.3389/fnins.2019.00532
7. Ilieva H, Polymenidou M, Cleveland DW. Non-cell autonomous toxicity in neurodegenerative disorders: ALS and beyond. J Cell Biol. 2009;187(6):761–72. https://doi.org/10.1083/jcb.200908164
8. García-Morales V, Rodríguez-Bey G, Gómez-Pérez L, Domínguez-Vías G, González-Forero D, Portillo F, et al. Sp1-regulated expression of p11 contributes to motor neuron degeneration by membrane insertion of TASK1. Nat Commun. 2019;10:3784
9. Devlin AC, Burr K, Borooah S, Foster JD, Cleary EM, Geti I, et al. Human iPSC-derived motoneurons harbouring TARDBP or C9ORF72 ALS mutations are dysfunctional despite maintaining viability. Nat Commun. 2015;6:5999. https://doi.org/10.1038/ncomms6999
10. Kim J, Hughes EG, Shetty AS, Arlotta P, Goff LA, Bergles DE, et al. Changes in the excitability of neocortical neurons in a mouse model of amyotrophic lateral sclerosis are not specific to corticospinal neurons and are modulated by advancing disease. J Neurosci. 2017;37(37):9037–53. https://doi.org/10.1523/jneurosci.0811-17.2017
11. Leroy F, Lamotte d'Incamps B, Imhoff-Manuel RD, Zytnicki D. Early intrinsic hyperexcitability does not contribute to motoneuron degeneration in amyotrophic lateral sclerosis. eLife. 2014;3:e04046. https://doi.org/10.7554/eLife.04046
12. Saxena S, Roselli F, Singh K, Leptien K, Julien JP, Gros-Louis F, et al. Neuroprotection through excitability and mTOR required in ALS motoneurons to delay disease and extend survival. Neuron. 2013;80(1):80–96. https://doi.org/10.1016/j.neuron.2013.07.027
13. Martinez-Silva ML, Imhoff-Manuel RD, Sharma A, Heckman CJ, Shneider NA, Roselli F, et al. Hypoexcitability precedes denervation in the large fast-contracting motor units in two unrelated mouse models of ALS. eLife. 2018;7:e30955. https://doi.org/10.7554/eLife.30955.
14. Lee HY, Murata J, Clair T, Polymeropoulos MH, Torres R, Manrow RE, et al. Cloning, chromosomal localization, and tissue expression of autotaxin from human teratocarcinoma cells. Biochem Biophys Res Commun. 1996;218(3):714–9. https://doi.org/10.1006/bbrc.1996.0127.

15. Herr DR, Chew WS, Satish RL, Ong WY. Pleotropic roles of autotaxin in the nervous system present opportunities for the development of novel therapeutics for neurological diseases. Mol Neurobiol. 2020;57:372–92. https://doi.org/10.1007/s12035-019-01719-1

16. Hanrieder J, Ewing AG. Spatial elucidation of spinal cord lipid- and metabolite- regulations in amyotrophic lateral sclerosis. Sci Rep. 2014;4:5266. https://doi.org/10.1038/srep05266

17. Blasco H, Veyrat-Durebex C, Bocca C, Patin F, Vourc'h P, Kouassi Nzoughet J, et al. Lipidomics reveals cerebrospinal-fluid signatures of ALS. Sci Rep. 2017;7(1):17652. https://doi.org/10.1038/s41598-017-17389-9

18. Lee JC, Park SM, Kim IY, Sung H, Seong JK, Moon MH. High-fat diet-induced lipidome perturbations in the cortex, hippocampus, hypothalamus, and olfactory bulb of mice. Biochim Biophys Acta Mol Cell Biol Lipids. 2018;1863(9):980–90. https://pubmed.ncbi.nlm.nih.gov/29787912/

19. Rancoule C, Dusaulcy R, Treguer K, Gres S, Attane C, Saulnier-Blache JS. Involvement of autotaxin/lysophosphatidic acid signaling in obesity and impaired glucose homeostasis. Biochimie. 2014;96:140–3. https://doi.org/10.1016/j.biochi.2013.04.010

20. Ning P, Yang B, Li S, Mu X, Shen Q, Hu F, et al. Systematic review of the prognostic role of body mass index in amyotrophic lateral sclerosis. Amyotroph Lateral Scler Front Degener. 2019;20(5–6):356–67. https://doi.org/10.1080/21678421.2019.1587631

21. García-Morales V, Montero F, González-Forero D, Rodríguez-Bey G, Gómez-Pérez L, Medialdea-Wandossell MJ, et al. Membrane-derived phospholipids control synaptic neurotransmission and plasticity. PLoS Biol. 2015;13(5):e1002153.

22. Gento-Caro Á, Vilches-Herrando E, García-Morales V, Portillo F, Rodríguez-Bey G, González-Forero D, et al. Interfering with lysophosphatidic acid receptor edg2/lpa$_1$ signalling slows down disease progression in *SOD1-G93A* transgenic mice. Neuropathol Appl Neurobiol. 2021;nan.12699. https://doi.org/10.1111/nan.12699.

23. Kress GJ, Dowling MJ, Meeks JP, Mennerick S. High threshold, proximal initiation, and slow conduction velocity of action potentials in dentate granule neuron mossy fibers. J Neurophysiol. 2008;100(1):281–91. https://pubmed.ncbi.nlm.nih.gov/18480368/

24. Portillo F, Moreno-López B. Nitric oxide controls excitatory/inhibitory balance in the hypoglossal nucleus during early postnatal development. Brain Struct Funct. 2020;225(9):2871–84. https://pubmed.ncbi.nlm.nih.gov/33130922/

25. Bannai H, Lévi S, Schweizer C, Inoue T, Launey T, Racine V, et al. Activity-dependent tuning of inhibitory neurotransmission based on GABAAR diffusion dynamics. Neuron. 2009;62(5):670–82. https://pubmed.ncbi.nlm.nih.gov/19524526/

26. Gierse J, Thorarensen A, Beltey K, Bradshaw-Pierce E, Cortes-Burgos L, Hall T, et al. A novel autotaxin inhibitor reduces lysophosphatidic acid levels in plasma and the site of inflammation. J Pharmacol Exp Ther. 2010;334(1):310–7. https://doi.org/10.1124/jpet.110.165845

27. Pan HL, Liu BL, Lin W, Zhang YQ. Modulation of Nav1.8 by lysophosphatidic acid in the induction of bone cancer pain. Neurosci Bull. 2016;32(5):445–54. https://pubmed.ncbi.nlm.nih.gov/27631681/

28. Roselli F, Caroni P. From intrinsic firing properties to selective neuronal vulnerability in neurodegenerative diseases. Neuron. 2015;85(5):901–10. https://doi.org/10.1016/j.neuron.2014.12.063

29. Saxena S, Caroni P. Selective neuronal vulnerability in neurodegenerative diseases: from stressor thresholds to degeneration. Neuron. 2011;71(1):35–48. https://doi.org/10.1016/j.neuron.2011.06.031

30. Thalman C, Horta G, Qiao L, Endle H, Tegeder I, Cheng H, et al. Synaptic phospholipids as a new target for cortical hyperexcitability and E/I balance in psychiatric disorders. Mol Psychiatry. 2018;23(8):1699–710. https://doi.org/10.1038/s41380-018-0053-1

31. Perrakis A, Moolenaar WH. Autotaxin: structure-function and signaling. J Lipid Res. 2014;55(6):1010–8. https://doi.org/10.1194/jlr.R046391

32. Talley EM, Solorzano G, Lei Q, Kim D, Bayliss DA. Cns distribution of members of the two-pore-domain (KCNK) potassium channel family. J Neurosci. 2001;21(19):7491–505. http://www.ncbi.nlm.nih.gov/pubmed/11567039?dopt=Citation

33. van Meeteren LA, Ruurs P, Storelers C, Bouwman P, van Rooijen MA, Pradere JP, et al. Autotaxin, a secreted lysophospholipase D, is essential for blood vessel formation during development. Mol Cell Biol. 2006;26(13):5015–22. https://doi.org/10.1128/mcb.02419-05

34. Tanaka M, Okudaira S, Kishi Y, Ohkawa R, Iseki S, Ota M, et al. Autotaxin stabilizes blood vessels and is required for embryonic vasculature by producing lysophosphatidic acid. J Biol Chem. 2006;281(35):25822–30. https://doi.org/10.1074/jbc.M605142200

35. Inoue M, Ma L, Aoki J, Ueda H. Simultaneous stimulation of spinal NK1 and NMDA receptors produces LPC which undergoes ATX-mediated conversion to LPA, an initiator of neuropathic pain. J Neurochem. 2008;107(6):1556–65. https://doi.org/10.1111/j.1471-4159.2008.05725.x

36. Lewandowski SA, Fredriksson L, Lawrence DA, Eriksson U. Pharmacological targeting of the PDGF-CC signaling pathway for blood-brain barrier restoration in neurological disorders. Pharmacol Ther. 2016;167:108–19. https://doi.org/10.1016/j.pharmthera.2016.07.016

37. Tigyi G, Hong L, Yakubu M, Parfenova H, Shibata M, Leffler CW. Lysophosphatidic acid alters cerebrovascular reactivity in piglets. Am J Physiol. 1995;268(5 Pt 2):H2048–55

38. Tigyi GJ, Yue J, Norman DD, Szabo E, Balogh A, Balazs L, et al. Regulation of tumor cell – Microenvironment interaction in the autotaxin-lysophosphatidic acid receptor axis. Adv Biol Regul. 2019;71:183–93. https://pubmed.ncbi.nlm.nih.gov/30243984/

39. Singh S, Singh TG. role of nuclear factor kappa B (NF-κB) signalling in neurodegenerative diseases: an mechanistic approach. Curr Neuropharmacol. 2020;18(10):918–35. https://pubmed.ncbi.nlm.nih.gov/32031074/

40. Gomes C, Cunha C, Nascimento F, Ribeiro JA, Vaz AR, Brites D. Cortical neurotoxic astrocytes with early ALS pathology and miR-146a deficit replicate gliosis markers of symptomatic SOD1G93A mouse model. Mol Neurobiol. 2019;56(3):2137–58. https://pubmed.ncbi.nlm.nih.gov/29995256/

41. Dutta K, Thammisetty SS, Boutej H, Bareil C, Julien JP. Mitigation of ALS pathology by neuron-specific inhibition of nuclear factor kappa B signaling. J Neurosci. 2020;40(26):5137–54. https://pubmed.ncbi.nlm.nih.gov/32457070/

42. Shibata N, Kakita A, Takahashi H, Ihara Y, Nobukuni K, Fujimura H, et al. Increased expression and activation of cytosolic phospholipase A2 in the spinal cord of patients with sporadic amyotrophic lateral sclerosis. Acta Neuropathol. 2010;119(3):345–54. https://doi.org/10.1007/s00401-009-0636-7

43. Kiaei M, Kipiani K, Petri S, Choi DK, Chen J, Calingasan NY, et al. Integrative role of cPLA with COX-2 and the effect of non-steriodal anti-inflammatory drugs in a transgenic mouse model of amyotrophic lateral sclerosis. J Neurochem. 2005;93(2):403–11. https://doi.org/10.1111/j.1471-4159.2005.03024.x

44. Sundaram JR, Chan ES, Poore CP, Pareek TK, Cheong WF, Shui G, et al. Cdk5/p25-induced cytosolic PLA2-mediated lysophosphatidylcholine production regulates neuroinflammation and triggers neurodegeneration. J Neurosci. 2012;32(3):1020–34. https://doi.org/10.1523/jneurosci.5177-11.2012

45. Solomonov Y, Hadad N, Levy R. Reduction of cytosolic phospholipase A2alpha upregulation delays the onset of symptoms in SOD1G93A mouse model of amyotrophic lateral sclerosis. J Neuroinflammation. 2016;13(1):134. https://doi.org/10.1186/s12974-016-0602-y

46. Tan Z, Lei H, Guo M, Chen Y, Zhai X. An updated patent review of autotaxin inhibitors (2017–present). Expert Opin Ther Pat. 2021;31(5):421–34. https://pubmed.ncbi.nlm.nih.gov/33342311/

SUPPORTING INFORMATION

Additional Supporting Information may be found in the online version of the article at the publisher's website.

FIGURE S1 Characterization of primary cultures of SMNs. (A) A high-magnification confocal image of SMNs at 6 days after platting immunolabelled for the MN marker SMI32. (B) Confocal images of SMNs, at the same time in culture, double labelled for SMI32 (green) and the nuclear marker DAPI (blue). Note that all nuclei in the field belong to SMI32-positive neurons. Scale bars: (A) 25 μm, (B) 100 μm